

Determination of B_d^0 - \bar{B}_d^0 mixing rate from the time evolution of dilepton events at the $\Upsilon(4S)$

The Belle Collaboration

Abstract

We report a determination of the B_d^0 - \bar{B}_d^0 mixing parameter Δm_d from the time evolution of dilepton yields in $\Upsilon(4S)$ decays. Data were collected by the Belle detector at KEKB. The proper-time difference distributions for same-sign and opposite-sign dilepton events were simultaneously fitted to an expression containing Δm_d as a free parameter. Both muons and electrons were used in the analysis. We obtain $\Delta m_d = 0.456 \pm 0.008$ (stat.) ± 0.030 (sys.) ps^{-1} (preliminary). This is the first determination of Δm_d from time evolution using $\Upsilon(4S)$ decays.

Typeset using REVTeX

A. Abashian⁴⁴, K. Abe⁸, K. Abe³⁶, I. Adachi⁸, Byoung Sup Ahn¹⁴, H. Aihara³⁷,
 M. Akatsu¹⁹, G. Alimonti⁷, K. Aoki⁸, K. Asai²⁰, M. Asai⁹, Y. Asano⁴², T. Aso⁴¹,
 V. Aulchenko², T. Aushev¹², A. M. Bakich³³, E. Banas¹⁵, S. Behari⁸, P. K. Behera⁴³,
 D. Beilene², A. Bondar², A. Bozek¹⁵, T. E. Browder⁷, B. C. K. Casey⁷, P. Chang²³,
 Y. Chao²³, B. G. Cheon³², S.-K. Choi⁶, Y. Choi³², Y. Doi⁸, J. Dragic¹⁷, A. Drutskoy¹²,
 S. Eidelman², Y. Enari¹⁹, R. Enomoto^{8,10}, C. W. Everton¹⁷, F. Fang⁷, H. Fujii⁸,
 K. Fujimoto¹⁹, Y. Fujita⁸, C. Fukunaga³⁹, M. Fukushima¹⁰, A. Garmash^{2,8}, A. Gordon¹⁷,
 K. Gotow⁴⁴, H. Guler⁷, R. Guo²¹, J. Haba⁸, T. Haji⁴, H. Hamasaki⁸, K. Hanagaki²⁹,
 F. Handa³⁶, K. Hara²⁷, T. Hara²⁷, T. Haruyama⁸, N. C. Hastings¹⁷, K. Hayashi⁸,
 H. Hayashii²⁰, M. Hazumi²⁷, E. M. Heenan¹⁷, Y. Higashi⁸, Y. Higashino¹⁹, I. Higuchi³⁶,
 T. Higuchi³⁷, T. Hirai³⁸, H. Hirano⁴⁰, M. Hirose¹⁹, T. Hojo²⁷, Y. Hoshi³⁵, K. Hoshina⁴⁰,
 W.-S. Hou²³, S.-C. Hsu²³, H.-C. Huang²³, Y.-C. Huang²¹, S. Ichizawa³⁸, Y. Igarashi⁸,
 T. Iijima⁸, H. Ikeda⁸, K. Ikeda²⁰, K. Inami¹⁹, Y. Inoue²⁶, A. Ishikawa¹⁹, R. Itoh⁸,
 G. Iwai²⁵, M. Iwai⁸, H. Iwasaki⁸, Y. Iwasaki⁸, D. J. Jackson²⁷, P. Jalocha¹⁵, H. K. Jang³¹,
 M. Jones⁷, R. Kagan¹², H. Kakuno³⁸, J. Kaneko³⁸, J. H. Kang⁴⁵, J. S. Kang¹⁴,
 P. Kapusta¹⁵, K. Kasami⁸, N. Katayama⁸, H. Kawai³, M. Kawai⁸, N. Kawamura¹,
 T. Kawasaki²⁵, H. Kichimi⁸, D. W. Kim³², Heejong Kim⁴⁵, H. J. Kim⁴⁵, Hyunwoo Kim¹⁴,
 S. K. Kim³¹, K. Kinoshita⁵, S. Kobayashi³⁰, S. Koike⁸, Y. Kondo⁸, H. Konishi⁴⁰,
 K. Korotushenko²⁹, P. Krokovny², R. Kulasiri⁵, S. Kumar²⁸, T. Kuniya³⁰, E. Kurihara³,
 A. Kuzmin², Y.-J. Kwon⁴⁵, M. H. Lee⁸, S. H. Lee³¹, C. Leonidopoulos²⁹, H.-B. Li¹¹,
 R.-S. Lu²³, Y. Makida⁸, A. Manabe⁸, D. Marlow²⁹, T. Matsubara³⁷, T. Matsuda⁸,
 S. Matsui¹⁹, S. Matsumoto⁴, T. Matsumoto¹⁹, K. Misono¹⁹, K. Miyabayashi²⁰,
 H. Miyake²⁷, H. Miyata²⁵, L. C. Moffitt¹⁷, G. R. Moloney¹⁷, G. F. Moorhead¹⁷,
 N. Morgan⁴⁴, S. Mori⁴², T. Mori⁴, A. Murakami³⁰, T. Nagamine³⁶, Y. Nagasaka¹⁸,
 Y. Nagashima²⁷, T. Nakadaira³⁷, T. Nakamura³⁸, E. Nakano²⁶, M. Nakao⁸, H. Nakazawa⁴,
 J. W. Nam³², S. Narita³⁶, Z. Natkaniec¹⁵, K. Neichi³⁵, S. Nishida¹⁶, O. Nitoh⁴⁰,
 S. Noguchi²⁰, T. Nozaki⁸, S. Ogawa³⁴, R. Ohkubo⁸, T. Ohshima¹⁹, Y. Ohshima³⁸,
 T. Okabe¹⁹, T. Okazaki²⁰, S. Okuno¹³, S. L. Olsen⁷, W. Ostrowicz¹⁵, H. Ozaki⁸,
 P. Pakhlov¹², H. Palka¹⁵, C. S. Park³¹, C. W. Park¹⁴, H. Park¹⁴, L. S. Peak³³, M. Peters⁷,
 L. E. Piiilonen⁴⁴, E. Prebys²⁹, J. Raaf⁵, J. L. Rodriguez⁷, N. Root², M. Rozanska¹⁵,
 K. Rybicki¹⁵, J. Ryuko²⁷, H. Sagawa⁸, Y. Sakai⁸, H. Sakamoto¹⁶, H. Sakaue²⁶,
 M. Satapathy⁴³, N. Sato⁸, A. Satpathy^{8,5}, S. Schrenk⁴⁴, S. Semenov¹², Y. Settai⁴,
 M. E. Sevier¹⁷, H. Shibuya³⁴, B. Shwartz², A. Sidorov², V. Sidorov², S. Stanić⁴², A. Sugi¹⁹,
 A. Sugiyama¹⁹, K. Sumisawa²⁷, T. Sumiyoshi⁸, J. Suzuki⁸, J.-I. Suzuki⁸, K. Suzuki³,
 S. Suzuki¹⁹, S. Y. Suzuki⁸, S. K. Swain⁷, H. Tajima³⁷, T. Takahashi²⁶, F. Takasaki⁸,
 M. Takita²⁷, K. Tamai⁸, N. Tamura²⁵, J. Tanaka³⁷, M. Tanaka⁸, Y. Tanaka¹⁸,
 G. N. Taylor¹⁷, Y. Teramoto²⁶, M. Tomoto¹⁹, T. Tomura³⁷, S. N. Tovey¹⁷, K. Trabelsi⁷,
 T. Tsuboyama⁸, Y. Tsujita⁴², T. Tsukamoto⁸, T. Tsukamoto³⁰, S. Uehara⁸, K. Ueno²³,
 N. Ujiie⁸, Y. Unno³, S. Uno⁸, Y. Ushiroda¹⁶, Y. Usov², S. E. Vahsen²⁹, G. Varner⁷,
 K. E. Varvell³³, C. C. Wang²³, C. H. Wang²², M.-Z. Wang²³, T.-J. Wang¹¹, Y. Watanabe³⁸,
 E. Won³¹, B. D. Yabsley⁸, Y. Yamada⁸, M. Yamaga³⁶, A. Yamaguchi³⁶, H. Yamaguchi⁸,
 H. Yamamoto⁷, H. Yamaoka⁸, Y. Yamaoka⁸, Y. Yamashita²⁴, M. Yamauchi⁸, S. Yanaka³⁸,
 M. Yokoyama³⁷, K. Yoshida¹⁹, Y. Yusa³⁶, H. Yuta¹, C.-C. Zhang¹¹, H. W. Zhao⁸,
 Y. Zheng⁷, V. Zhilich², and D. Žontar⁴²

¹Aomori University, Aomori

- ²Budker Institute of Nuclear Physics, Novosibirsk
- ³Chiba University, Chiba
- ⁴Chuo University, Tokyo
- ⁵University of Cincinnati, Cincinnati, OH
- ⁶Gyeongsang National University, Chinju
- ⁷University of Hawaii, Honolulu HI
- ⁸High Energy Accelerator Research Organization (KEK), Tsukuba
- ⁹Hiroshima Institute of Technology, Hiroshima
- ¹⁰Institute for Cosmic Ray Research, University of Tokyo, Tokyo
- ¹¹Institute of High Energy Physics, Chinese Academy of Sciences, Beijing
- ¹²Institute for Theoretical and Experimental Physics, Moscow
- ¹³Kanagawa University, Yokohama
- ¹⁴Korea University, Seoul
- ¹⁵H. Niewodniczanski Institute of Nuclear Physics, Krakow
- ¹⁶Kyoto University, Kyoto
- ¹⁷University of Melbourne, Victoria
- ¹⁸Nagasaki Institute of Applied Science, Nagasaki
- ¹⁹Nagoya University, Nagoya
- ²⁰Nara Women's University, Nara
- ²¹National Kaohsiung Normal University, Kaohsiung
- ²²National Lien-Ho Institute of Technology, Miao Li
- ²³National Taiwan University, Taipei
- ²⁴Nihon Dental College, Niigata
- ²⁵Niigata University, Niigata
- ²⁶Osaka City University, Osaka
- ²⁷Osaka University, Osaka
- ²⁸Panjab University, Chandigarh
- ²⁹Princeton University, Princeton NJ
- ³⁰Saga University, Saga
- ³¹Seoul National University, Seoul
- ³²Sungkyunkwan University, Suwon
- ³³University of Sydney, Sydney NSW
- ³⁴Toho University, Funabashi
- ³⁵Tohoku Gakuin University, Tagajo
- ³⁶Tohoku University, Sendai
- ³⁷University of Tokyo, Tokyo
- ³⁸Tokyo Institute of Technology, Tokyo
- ³⁹Tokyo Metropolitan University, Tokyo
- ⁴⁰Tokyo University of Agriculture and Technology, Tokyo
- ⁴¹Toyama National College of Maritime Technology, Toyama
- ⁴²University of Tsukuba, Tsukuba
- ⁴³Utkal University, Bhubaneswer
- ⁴⁴Virginia Polytechnic Institute and State University, Blacksburg VA
- ⁴⁵Yonsei University, Seoul

I. INTRODUCTION

The phenomenon of B_d^0 - \bar{B}_d^0 mixing is a manifestation of higher-order box diagrams in the standard model, and its rate is regarded as a fundamental parameter of the B meson system. The observed value should be well described by the standard model and is proportional to $|V_{tb}^* V_{td}|^2$ if the top-quark loop is the dominant contribution. B_d^0 - \bar{B}_d^0 mixing is also a source of CP violation in B_d^0 decays into CP eigenstates, and a precise determination of the mixing parameter Δm_d is necessary to make precise measurements of any CP asymmetries. The parameter Δm_d has been measured by LEP experiments [1], CDF [2], and SLD [3] from the time evolution of B_d^0 meson decays, while ARGUS and CLEO have measured it using the integrated fraction of same-flavor B pair decays in $\Upsilon(4S)$ events [4,5]. In the last two experiments the B_d^0 mesons are produced nearly at rest, and a time-dependent measurement is not possible.

In this paper, we determine Δm_d from the time evolution of same-sign (SS) and opposite-sign (OS) dilepton yields in $\Upsilon(4S)$ decays created by the KEKB asymmetric e^+e^- colliding beam accelerator [6]. KEKB employs an 8.0 GeV electron beam and a 3.5 GeV positron beam, resulting in a center of mass moving along the electron beam direction with a Lorentz boost of $\gamma\beta = 0.425$. Consequently, the decay vertices of the two B mesons are typically separated by $200\mu\text{m}$, a distance large enough to be measured by a silicon vertex detector. High-momentum leptons can be used for tagging the B flavor. Combining this information allows us to measure the time evolution of the dileptons from $\Upsilon(4S)$ decays, which in turn permits us to determine the mixing parameter with little ambiguity.

The time evolution of same-flavor ($B_d^0 B_d^0$, $\bar{B}_d^0 \bar{B}_d^0$) and opposite-flavor ($B_d^0 \bar{B}_d^0$) decays given a $B_d^0 \bar{B}_d^0$ initial state are given by

$$N_{same} \propto e^{-|\Delta t|/\tau_{B_d^0}} [1 - \cos(\Delta m_d \Delta t)], \quad (1)$$

$$N_{opp} \propto e^{-|\Delta t|/\tau_{B_d^0}} [1 + \cos(\Delta m_d \Delta t)], \quad (2)$$

where Δm_d is the mass difference between the two mass eigenstates of the neutral B meson, $\tau_{B_d^0}$ is the average neutral B meson life time, and Δt is the proper time difference between the two B -meson decays.

II. BELLE DETECTOR AND DATA SAMPLE

The analysis presented here is based on samples of integrated luminosity 5.1 fb^{-1} taken at the $\Upsilon(4S)$ resonance and 0.6 fb^{-1} taken at an energy 50 to 60 MeV below the $\Upsilon(4S)$.

Belle [7] is a detector that makes precise measurements of charged and neutral particles over a wide acceptance.

The tracking of charged particles is done by a silicon vertex detector (SVD) and a central drift chamber (CDC) placed in a 1.5-T magnetic field, generated by a 3.4-m-diameter superconducting solenoid. The SVD consists of three layers of $300\text{-}\mu\text{m}$ -thick double-sided silicon strip detectors [8], surrounding a double-walled beryllium beam pipe of total thickness 1.0 mm and diameter 4.6 cm. The CDC is a small-cell cylindrical drift chamber operated with a He(50%)/Ethane(50%) gas mixture [9]. It consists of 50 anode layers, including 18 layers of small-angle stereo wires, which provide three-dimensional reconstruction of trajectories.

The innermost three layers have cathode-strip readout finely segmented in the z -direction. A Kalman filter method is used to determine tracking parameters by combining the CDC and SVD hits and taking into account the non-uniform magnetic field. Using muon tracks from cosmic rays and from $e^+e^- \rightarrow \mu^+\mu^-$, a resolution of $\sigma_{p_t}/p_t = (0.36 \oplus 0.28p_t)\%$, where p_t is the transverse momentum in GeV/ c , was obtained. The impact-parameter resolution at the interaction point is $(21 + 69/p\beta \sin^{3/2} \theta) \mu\text{m}$ in $r\phi$ and $(41 + 48/p\beta \sin^{5/2} \theta) \mu\text{m}$ in the z direction. The CDC covers the region of polar angle between 17 and 150 degrees in the laboratory system, where the polar angle is measured with respect to the direction opposite the 3.5 GeV positron beam. This corresponds to 92% of the 4π solid angle in the center-of-mass. The SVD covers the polar angle range between 21 and 140 degrees.

Located outside of the CDC, an array of 1188 aerogel Cerenkov counters (ACC), and 128 time-of-flight (TOF) scintillation counters provide particle identification together with dE/dx measurements by the CDC. The dE/dx resolution for hadron tracks is 6.9%. The TOF provides a time resolution of ~ 100 ps [10]. The ACC modules have indices of refraction ranging from 1.01 to 1.03, depending on the polar angle [11]. The index varies to match the kinematics of decay products from boosted B mesons.

The energies and positions of photons and electrons are measured by an array of 8736 CsI crystals (ECL) [12] situated just inside the solenoid and end yokes. The energy resolution is $\sigma_E/E = (1.3 \oplus 0.07/E \oplus 0.8/E^{1/4})\%$, where E is in GeV. The ECL covers the same angular region as the CDC.

The iron return yoke comprises 14 layers of 4.7-cm-thick iron plates separated by gaps containing resistive plate counters (RPCs). This system, called KLM, is used to measure the trajectories of muons penetrating the iron and the interactions of K_L particles [13]. The KLM covers the polar angle region between 20 and 155 degrees.

III. DATA ANALYSIS

A. Selection of Hadronic Events

Hadronic events were selected based on quantities calculated using well reconstructed tracks and clusters. Tracks were required to satisfy $P_t > 0.1$ GeV/ c , $|dr| < 2.0$ cm, and $|dz| < 4.0$ cm, where dr is the distance of nearest approach of the track to the z -axis and dz is the z -position of the track at the near point. Cluster energies were required to be larger than 0.1 GeV. All four-momenta were boosted to the center-of-mass (CM) frame, assuming that all charged tracks have the pion mass and all unmatched ECL clusters have zero mass. Events were then required to satisfy the following conditions:

1. number of tracks ≥ 5 ,
2. primary event vertex satisfies $V_r < 1.5$ cm and $|V_z| < 3.5$ cm,
3. $E_{\text{vis}} \geq 0.5W$,
4. $|\Sigma p_z| \leq 0.3W$,
5. $0.025W \leq \Sigma E_{\text{ECL}} \leq 0.9W$,

6. the ratio R_2 of the second and zeroth Fox-Wolfram moments [14] satisfies $R_2 \leq 0.7$.

Here E_{vis} is the total visible energy detected by the ECL and CDC; W/c^2 is the $\Upsilon(4S)$ mass; p_z is the z component of the net reconstructed momentum; E_{ECL} is the energy deposited in the ECL. The radial and z coordinates of the primary event, V_r and V_z , were obtained by fitting tracks to a common vertex. There are 14.1 million events that satisfy the above criteria.

Off-resonance data were used to determine the fraction of continuum events in the selected hadronic events. Based on this analysis we combined generated $B\bar{B}$ and continuum Monte Carlo event samples in the ratio of 1:3.66 for simulations of background.

B. Lepton Identification

Electrons

For electron identification (in what follows “electron” should be taken to mean “electron and positron”), we used the position, cluster energy, and shape of the shower in the ECL, together with the dE/dx measurement in the CDC and the hit information of the ACC to construct a likelihood function to discriminate between electron and non-electron (mainly hadron) tracks. This provided a $\sim 90\%$ efficiency for electron tracks and a $\sim 0.5\%$ misidentification probability for hadron tracks with momentum above 1 GeV/ c .

In order to reduce electrons from γ conversion, the pair invariant mass $M_{e^+e^-}$ was calculated for all combinations of an electron candidate and an oppositely charged track. If for any pair $M_{e^+e^-}$ was less than 100 MeV/ c^2 , the electron candidate was rejected.

Muons

Muon identification is based on the KLM hits associated with charged tracks from the CDC extrapolated through the ECL, solenoid, and iron return yoke. A variable taking into account the range of the tracks and the matching quality of the hits was constructed and used to discriminate between muon and hadron tracks. The efficiency is estimated to be $\sim 85\%$ for muon tracks with a momentum above 1 GeV/ c , and the misidentification probability is $\sim 2\%$.

C. Dilepton Selection

To reject events containing leptons from J/ψ decay the invariant mass was calculated for all combinations of each candidate lepton with oppositely charged tracks. Events containing combinations satisfying

$$\begin{aligned} & |M_{\mu^+\mu^-} - M_{J/\psi}| < 50 \text{ MeV}/c^2 \\ \text{or } & -150 < M_{e^+e^-} - M_{J/\psi} < 50 \text{ MeV}/c^2 \end{aligned}$$

were rejected (J/ψ -veto cut).

Among events passing this cut, dilepton event candidates were required to contain two or more leptons satisfying the criteria listed below.

1. The laboratory polar angle for each lepton was required to lie in the range $30^\circ < \theta < 135^\circ$.
2. The CM momentum for each lepton was required to lie in the range $1.1 \text{ GeV}/c < p^* < 2.3 \text{ GeV}/c$.
3. Each lepton track was required to satisfy $|dr^{\text{IP}}| < 0.05 \text{ cm}$ and $|dz^{\text{IP}}| < 2.0 \text{ cm}$. Here, dr^{IP} and dz^{IP} are the distances of closest approach to the run-dependent interaction point ($x^{\text{IP}}, y^{\text{IP}}, z^{\text{IP}}$), described below in more detail.
4. Tracks were required to have at least one associated SVD hit in the r - ϕ view and at least two associated SVD hits in the r - z view.
5. The opening angle between the leptons in the CM frame was required to satisfy $-0.8 < \cos \theta_{\ell\ell}^* < 0.95$. This served to reduce secondary leptons and fakes from the same B -mesons and from the continuum.

If more than two leptons were present, those with the highest and the second highest CM momentum were chosen.

The opening angle distributions prior to the application of the opening angle cut are shown in Figure 1. Figures 2 and 3 show the CM momentum distributions for selected dileptons. The contributions from various sources based on Monte Carlo simulation are also shown.

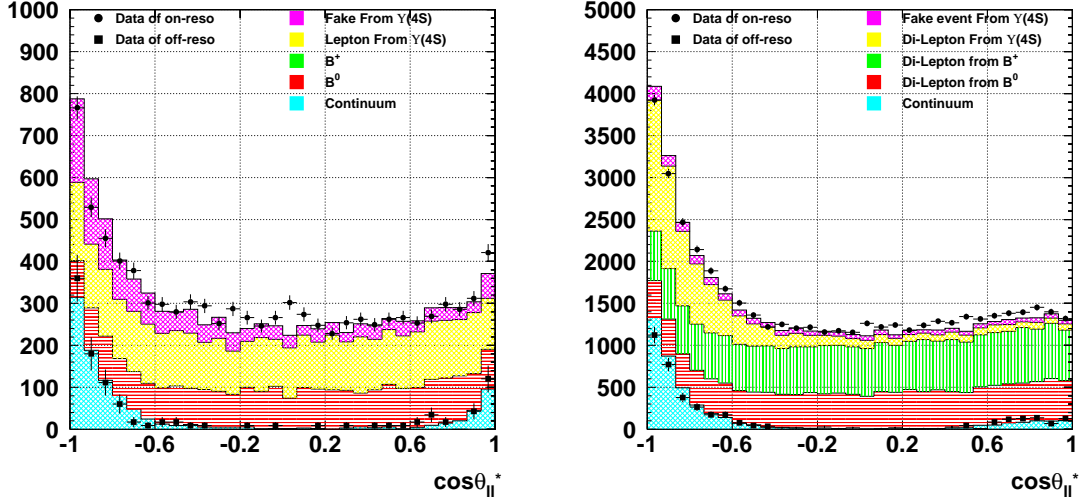


FIG. 1. Opening angle between the two leptons in the CM frame for same-sign (left) and opposite-sign (right) dileptons. The closed-circle points are for on-resonance data and the closed-square points are for off-resonance data normalized by the luminosity ratio. Histograms are Monte Carlo estimates from various sources.

Applying the criteria listed above yielded 7418 SS and 35633 OS dilepton events.

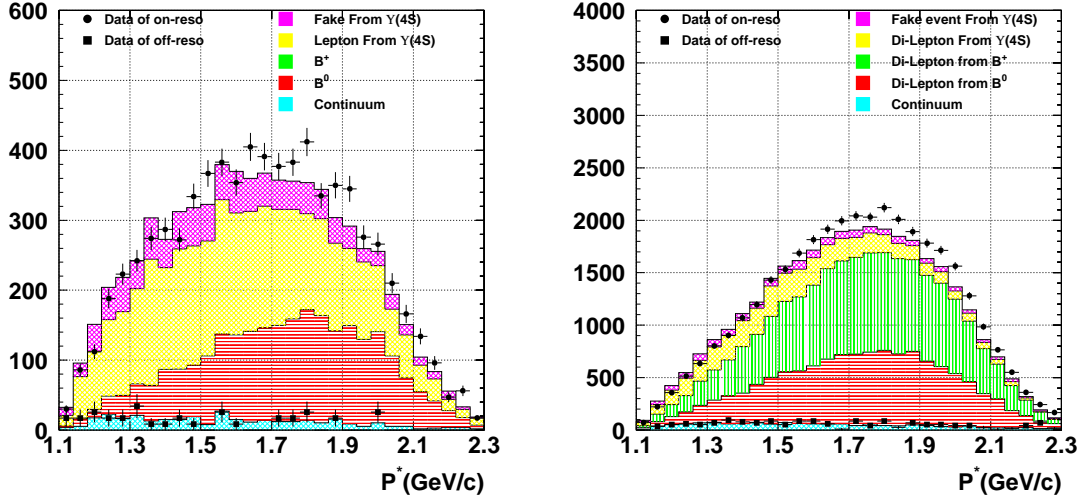


FIG. 2. CM momentum of the lepton with the higher momentum for selected dilepton events for same-sign (left) and opposite-sign (right) dileptons. Otherwise, same as Figure 1.

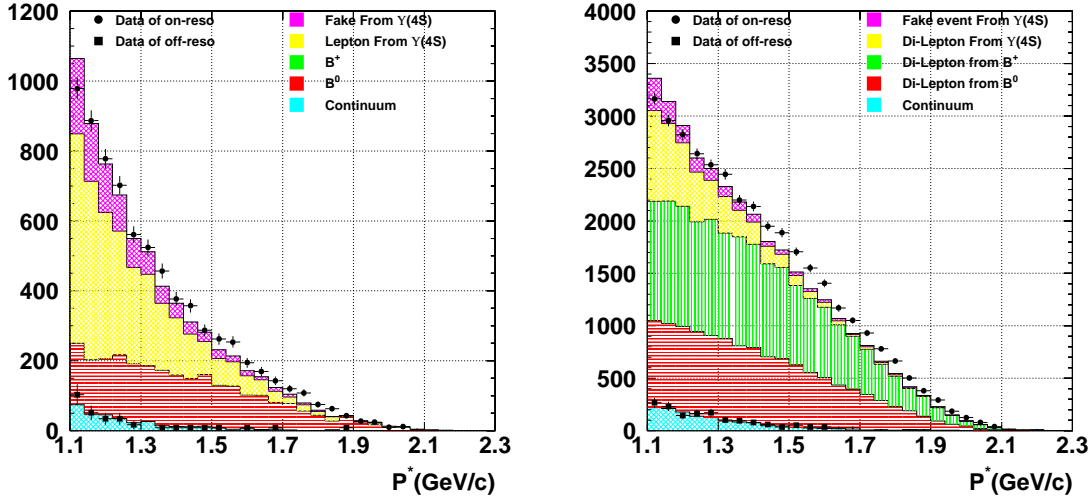


FIG. 3. CM momentum of the lepton with the lower momentum for selected dilepton events for same-sign (left) and opposite-sign (right) dileptons. Otherwise, same as Figure 1.

D. z -Vertex Determination and Proper-time Difference

Since the $\Upsilon(4S)$ is boosted along the z axis, the B meson travels a very short distance in the transverse (x and y) dimensions, and the difference in z -vertex position between the two leptons is a good measure of the difference in decay time between the two B mesons in an event.

The z -vertex position of each lepton was determined by finding the intersection of the fitted lepton tracks with the three-dimensional volume known to contain the B_d^0 decay vertices. The shape of this volume ($\sigma_x \simeq 100 \sim 120 \mu\text{m}$, $\sigma_y \simeq 20 \mu\text{m}$, $\sigma_z \simeq 2000 \sim 3000 \mu\text{m}$) is that of a highly elongated ellipsoid, rendering this procedure approximately equivalent to

finding the intersection of the lepton tracks with the (run-dependent) x - z plane.

For the B -meson decay-point profile in x and y , we used the run-dependent coordinates ($x^{\text{IP}}, y^{\text{IP}}$) of the interaction point and their widths

$$\begin{aligned}\sigma_x^2 &\simeq (\sigma_x^{\text{IP}})^2 + \sigma_B^2 \\ \sigma_y^2 &\simeq (\sigma_y^{\text{IP}})^2 + \sigma_B^2.\end{aligned}$$

Here, $\sigma_{x/y}^{\text{IP}}$ is the run-dependent size of the interaction point and σ_B is the transverse flight length of the B mesons for which we used $20 \mu\text{m}$, based on a Monte Carlo estimate.

Profile parameters for the interaction point are determined by the primary vertex position distribution of hadronic events. Since the y width of the true interaction-profile is $\sim 5 \mu\text{m}$, which is much smaller than the measurement resolution, the observed y width gives the experimental resolution. Typically, $\sigma_x^{\text{IP}} = 100\sim 120 \mu\text{m}$ and $\sigma_z^{\text{IP}} = 2\sim 3 \text{ mm}$. The variation in interaction position from run to run was about 1.2 mm, 0.3 mm, and 4 mm for the x , y , and z directions, respectively.

The proper-time difference was calculated from the z positions of the two lepton vertices using

$$\Delta t = \frac{\Delta z}{c\beta\gamma} \quad (3)$$

where $\Delta z = z_1 - z_2$ is the difference between the two z vertices, $\beta\gamma = 0.425$ is the Lorentz boost factor of the e^+e^- CM system. For OS events, the positively charged lepton is taken as the first lepton (z_1) and the negatively charged lepton as the second. For SS events the absolute value of Δz is used.

E. Determination of the Mixing Parameter

The mixing parameter Δm_d was extracted by simultaneously fitting the time evolution of the SS and OS dilepton samples to multiparameter functions which take into account both signal and backgrounds. The fit is constructed to vary both the oscillation period and the integrated rate as a function of Δm_d . A signal candidate is defined as one where both leptons are primary leptons from semileptonic decay of B_d^0 or B^\pm . Background candidates include at least one secondary or fake lepton, or they come from continuum events. The time evolution of the signal events may be described by well-known theoretical functions, whereas that of the background derives from many processes and cannot be described by theoretical formulas. For those, we rely on time-evolution descriptions obtained from Monte Carlo simulation of the background.

Simulated signal and background dilepton events were classified according to their origin: unmixed- B_d^0 pairs, mixed- B_d^0 pairs, B^+B^- , and continuum, as illustrated in Figure 4. Unmixed- and mixed- B_d^0 pairs were separated because their relative amounts and the shapes of their distributions depend on the mixing parameter.

The observed SS and OS dilepton proper-time distributions are described as the sum of the following contributions:

SS dileptons

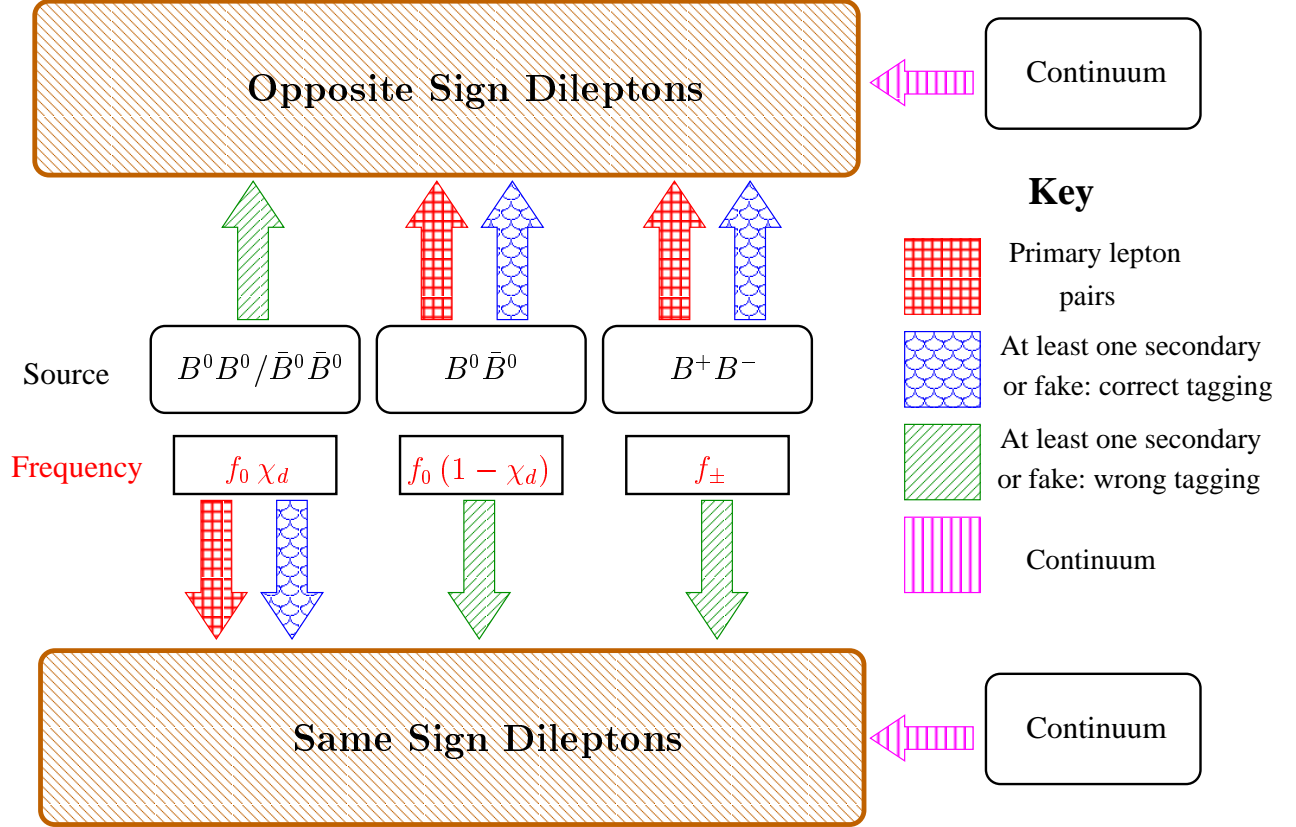


FIG. 4. Schematic picture of categorization of dilepton signals and backgrounds according their sources.

- signal dileptons from $B_d^0 \bar{B}_d^0$ or $\bar{B}_d^0 B_d^0$: $\eta_{\ell^\pm \ell^\pm}^{\text{mix}} P_{\ell^\pm \ell^\pm}^0(\Delta t) b_0^2 f_0 N_{\Upsilon(4S)}$
- background from $B_d^0 \bar{B}_d^0$ or $\bar{B}_d^0 B_d^0$ pairs: $\epsilon_{\text{SS}}^{\text{mix}} B_{\text{SS}}^{\text{mix}}(\Delta t) f_0 \chi_d N_{\Upsilon(4S)}$
- background from $B_d^0 \bar{B}_d^0$ pairs: $\epsilon_{\text{SS}}^{\text{unm}} B_{\text{SS}}^{\text{unm}}(\Delta t) f_0 (1 - \chi_d) N_{\Upsilon(4S)}$
- background from $B^+ B^-$ pairs: $\epsilon_{\text{SS}}^{\text{chgd}} B_{\text{SS}}^{\text{chgd}}(\Delta t) f_\pm N_{\Upsilon(4S)}$
- background from the continuum: $\epsilon_{\text{SS}}^{\text{cnt}} B_{\text{SS}}^{\text{cnt}}(\Delta t) N_{\text{cnt}}$

OS dileptons

- signal dileptons from $B_d^0 \bar{B}_d^0$ or $B^+ B^-$ pairs:
 $\eta_{\ell^+ \ell^-}^{\text{unm}} P_{\ell^+ \ell^-}^0(\Delta t) b_0^2 f_0 N_{\Upsilon(4S)} + \eta_{\ell^+ \ell^-}^{+-} P_{\ell^+ \ell^-}^{+-}(\Delta t) b_\pm^2 f_\pm N_{\Upsilon(4S)}$
- background from $B_d^0 \bar{B}_d^0$ or $\bar{B}_d^0 B_d^0$ pairs: $\epsilon_{\text{OS}}^{\text{mix}} B_{\text{OS}}^{\text{mix}}(\Delta t) f_0 \chi_d N_{\Upsilon(4S)}$
- background from $B_d^0 \bar{B}_d^0$ pairs: $\epsilon_{\text{OS}}^{\text{unm}} B_{\text{OS}}^{\text{unm}}(\Delta t) f_0 (1 - \chi_d) N_{\Upsilon(4S)}$
- background from $B^+ B^-$ pairs: $\epsilon_{\text{OS}}^{\text{chgd}} B_{\text{OS}}^{\text{chgd}}(\Delta t) f_\pm N_{\Upsilon(4S)}$
- background from the continuum: $\epsilon_{\text{OS}}^{\text{cnt}} B_{\text{OS}}^{\text{cnt}}(\Delta t) N_{\text{cnt}}$

Here, $N_{\Upsilon(4S)}$ and N_{cnt} are the number of $\Upsilon(4S)$ and continuum events selected by the hadronic cuts. f_0 and f_\pm are the branching fractions to neutral- and charged- B pairs of the $\Upsilon(4S)$ ($f_0 + f_\pm = 1$). b^0 and b^\pm are the semileptonic branching fractions of B_d^0 and B^\pm , respectively. The η 's are the selection efficiencies for signal dileptons of each category. The ϵ 's are the fractions of dilepton events selected from $N_{\Upsilon(4S)}$ or N_{cnt} events for each background category. χ_d is given by

$$\chi_d = \frac{x_d^2}{2(1 + x_d^2)} = \frac{\tau_{B_d^0}^2 \Delta m_d^2}{2(1 + \tau_{B_d^0}^2 \Delta m_d^2)}$$

$P(\Delta t)$'s and $B(\Delta t)$'s are the proper-time distributions for signal and background dilepton components.

The proper-time distribution for signal dileptons is given by the convolution of a theoretical function with the detector response function $g(\Delta t)$:

$$P_\alpha^\beta(\Delta t) = \int g(\Delta t - \Delta t') F_\alpha^\beta(\Delta t') d(\Delta t')$$

The theoretical functions are

$$F_{\ell^\pm \ell^\pm}^0(\Delta t) = \frac{1}{4\tau_{B_d^0}} e^{-|\Delta t|/\tau_{B_d^0}} [1 - \cos(\Delta m_d \Delta t)] \quad (4)$$

$$F_{\ell^+ \ell^-}^0(\Delta t) = \frac{1}{4\tau_{B_d^0}} e^{-|\Delta t|/\tau_{B_d^0}} [1 + \cos(\Delta m_d \Delta t)] \quad (5)$$

$$F_{\ell^+ \ell^-}^{+-}(\Delta t) = \frac{1}{2\tau_B^+} e^{-|\Delta t|/\tau_{B^+}} \quad (6)$$

1. Response Function

An accurate detector-response function, $g(\Delta t) = g(\Delta z/\beta\gamma c)$, is essential to obtaining a reliable fit to the data. A good approximation may be obtained from data by observing the Δz distribution for dileptons from J/ψ decays in data. These decays are found in the same dataset as was used in this analysis and have lepton momentum spectra close to those of primary leptons from B decays. Monte Carlo simulation shows good agreement between the dilepton response function and the Δz distribution of dileptons from J/ψ . Although in principle the dilepton response function for our data could have been derived from Monte Carlo, the current version of our simulation does not fully reproduce the data.

Dileptons from J/ψ decays were selected by applying the criteria described in Section III C on opposite-sign dileptons, but with the J/ψ -veto cut replaced by

$$|M_{\ell^+\ell^-} - M_{J/\psi}| < 40 \text{ MeV}/c^2.$$

The number of background events in the selected mass region was obtained by fitting the $\ell^+\ell^-$ mass distribution to the sum of a Gaussian and a linear function. The background was estimated and subtracted using the upper side band of the mass distribution. We did not include the lower side band due to the presence there of radiative decays, $J/\psi \rightarrow \ell^+\ell^-\gamma$. Fitting the Δz distribution obtained in this way to a single Gaussian function yields widths of $\sigma = 112 \mu\text{m}$ and $\sigma = 100 \mu\text{m}$, for data and Monte Carlo, respectively. The Monte Carlo distribution gives a good fit to data if it is given an “extra smearing” of $50 \mu\text{m}$, that is, it is convoluted with a Gaussian of $\sigma = 50 \mu\text{m}$. Figure 5 shows the Δz distributions obtained from J/ψ for data and Monte Carlo, without (a) and with (b) the extra smearing.

2. Background Distributions

Background dileptons for each of the above categories arise from various sources, which give different Δz distributions. These include mainly primary leptons paired with secondary leptons from c -quark or τ decays, or fake leptons originating from the same or different B 's. For the SS dileptons, the background is dominated by $B\bar{B}$ decays, where one lepton is a primary lepton and the other is from a $b \rightarrow c \rightarrow \ell$ decay. For the OS dileptons, the background consists mainly of primary and secondary leptons from the same B . Monte Carlo simulations were used to estimate the background distribution of each category. Since the size of the off-resonance sample is too small to give good statistical accuracy, we estimated the continuum contributions by Monte Carlo simulation as well.

From simulation and observation in data of dileptons from J/ψ decays, we know that the detector response function for data is not well reproduced by the current version of our simulation, but that a good fit is obtained through an additional Gaussian smearing of $50 \mu\text{m}$ (see Figure 5). We therefore applied the same smearing to each background distribution before including it for fitting to data. This procedure was verified by comparing the Δz distributions of lepton-kaon and lepton-pion pairs for data and Monte Carlo with the same smearing. The same kinematic cuts were imposed in selecting dileptons and lepton-hadron pairs. Good agreement between data and smeared Monte Carlo distributions was obtained.

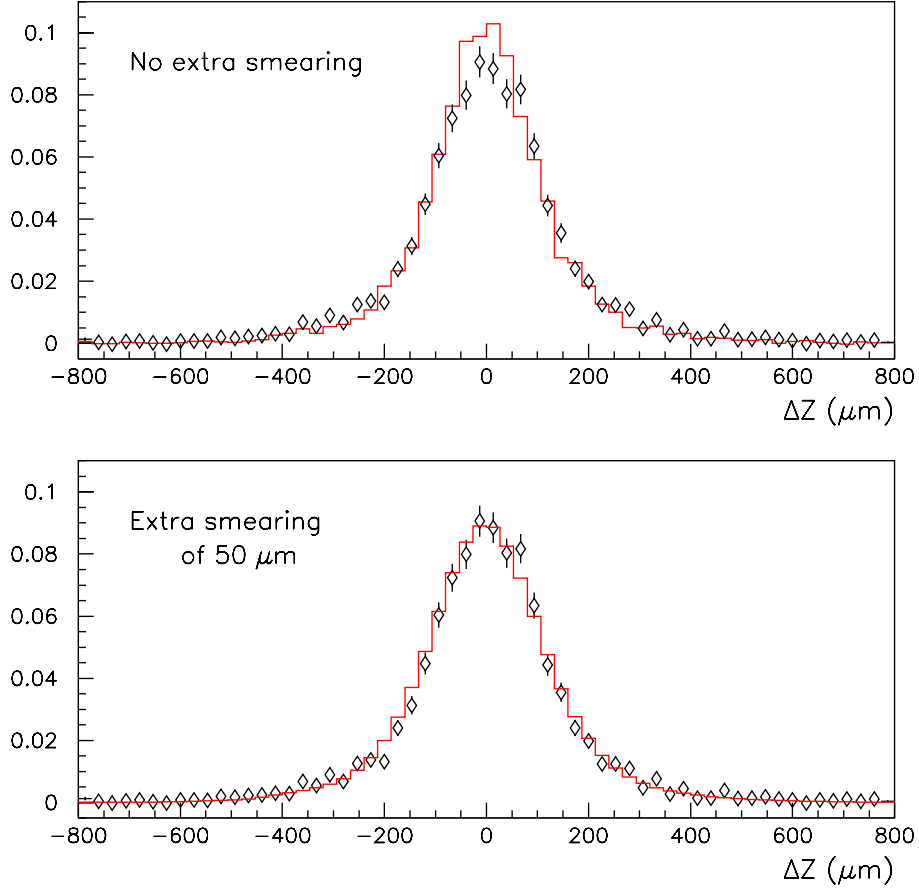


FIG. 5. Δz distribution for dileptons of J/ψ decays for the data (points) and Monte Carlo (histogram) without (top) and with (bottom) extra smearing.

Several aspects of the current Monte Carlo simulation contain known errors that have required adjustment of the background estimations. The fake rate of pions in electron and muon identification was measured using pions from $K_S \rightarrow \pi^+\pi^-$ decays and compared with Monte Carlo. We found differences of $10.4 \pm 6.1\%$ and $2 \pm 22\%$ in the overall fake rate for muons and electrons identification, respectively. We corrected the fake lepton contributions from the Monte Carlo for these differences. We also corrected the Monte Carlo secondary particle contributions from D^0 and D^\pm for differences between the inclusive branching ratios measured by CLEO [17] and those in the Monte Carlo generator.

F. Fitting and Results

We have developed two fitting methods to extract the mixing parameter from the Δz (proper-time) distribution of dileptons.

Method I

In this method, a binned maximum likelihood fit to the Δz distributions of the SS and OS dileptons was performed simultaneously. It was assumed that the relative fractions of the background components were correctly described by the Monte Carlo and that the Monte Carlo correctly described the relative selection efficiencies for signal dileptons.

The main parameter of the fit was Δm_d . The value $\tau_{B_d^0}$ was fixed to the world average value [15]. The relative ratios of the ϵ parameters (introduced in Section III E) were fixed to the values determined by Monte Carlo, as were the relative ratios of the η 's, but the ratio of the η 's and the ϵ 's was allowed to float.

The ratios $f_{\pm}/f_0 = 1.07$ [16], $\tau_{B^{\pm}}/\tau_{B_d^0} = 1.04$ [15], and $b_{\pm}/b_0 = \tau_{B^{\pm}}/\tau_{B_d^0}$ were fixed in the fit. This resulted in one free parameter in the fit besides Δm_d and the overall normalization. The dependence of the background shape $B_{\text{SS/OS}}^{\text{mix/unm}}(\Delta z)$ on Δm_d was approximated by linearly interpolating the distributions obtained for two mixing parameter values as

$$B(\Delta z; \Delta m_d) = (1 - \gamma)B(\Delta z; \Delta m_d = 0.423) + \gamma B(\Delta z; \Delta m_d = 0.464),$$

where $\gamma = (\Delta m_d - 0.423)/(0.464 - 0.423)$. Look-up tables were used for the response function and the background-distribution functions. The region of the fit was limited to $|\Delta z| < 1.85$ mm.

The fit yielded

$$\Delta m_d = 0.456 \pm 0.008 \text{ ps}^{-1}$$

with $\chi^2 = 342$ for 382 degrees of freedom. Figure 6 shows the Δz distributions for the data together with the fitted curves. Figure 7 shows the OS and SS asymmetry, $(N_{\text{OS}} - N_{\text{SS}})/(N_{\text{OS}} + N_{\text{SS}})$, for data together with the fitted result. In this figure, the negative Δz region for the opposite-sign dileptons is folded into the positive region for display purposes.

Method II

As a cross check, another type of fitting method, which differs from the first method in parameterization and other technical aspects, was employed. In this method, the background treatment was simplified, and its shape was estimated using $\Delta m_d = 0.464$ only. An unbinned maximum likelihood fit was performed with analytic functions both for the response function and for the background distributions. The response function was fitted to a double-Gaussian function. The background distributions were divided into several types according to the shape of their Δz distributions and the origin of the leptons. Each distribution was fitted to a double-Gaussian and summed according to the ratios obtained from Monte Carlo simulation. The difference of detector resolution between data and Monte Carlo simulation was taken into account in the same way as Method I.

The ratios f_{\pm}/f_0 , τ_{B_0} , $\tau_{B^{\pm}}/\tau_{B_d^0}$, b_{\pm}/b_0 were fixed to the same values used in Method I. The fractions of SS and OS backgrounds were taken as independent parameters in the fit. Therefore, there were two free parameters besides Δm_d in the fit. As in Method I, the fit region was limited to $|\Delta z| < 1.85$ mm.

The fit yielded

$$\Delta m_d = 0.450 \pm 0.013 \text{ ps}^{-1}$$

which is consistent with Method I.

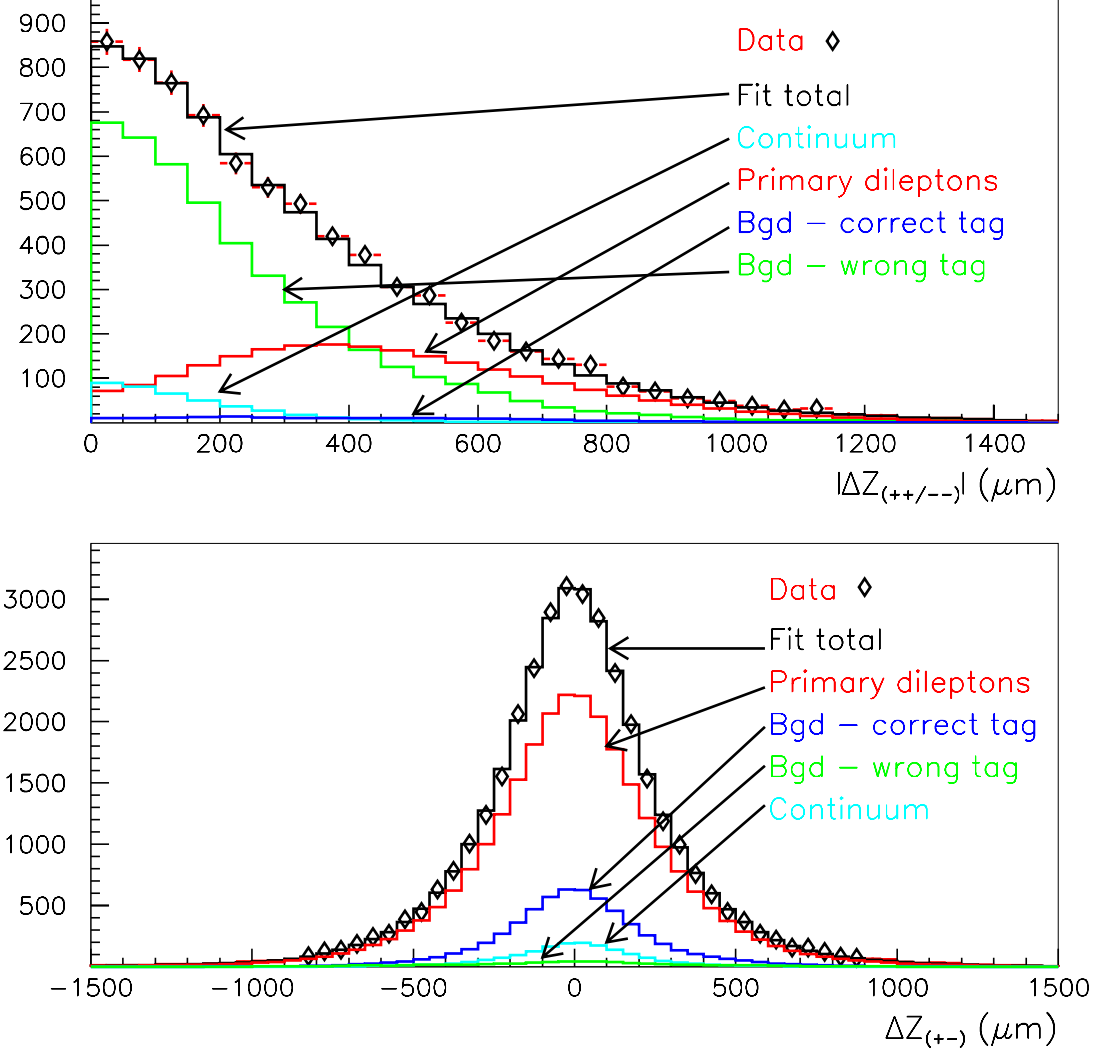


FIG. 6. Δz distribution of dileptons for data together with fit result. The upper plot shows the distributions for same-sign, and the lower plots for opposite-sign dileptons. Signal and background dileptons obtained from the fit are also shown.

G. Systematic Error

We examined the following contributions to the systematic error.

Uncertainties in f_0/f_{\pm} and the B_d^0 and B^{\pm} lifetimes

As mentioned previously, the values of f_0/f_{\pm} , $\tau_{B_d^0}$ and $\tau_{B^{\pm}}/\tau_{B_d^0}$ were fixed to their established central values [15,16]. Contributions to the systematic errors due to uncertainties in these were estimated by repeating fits after varying each by $\pm 1\sigma$. The variation of $\tau_{B^{\pm}}/\tau_{B_d^0}$ simultaneously changes the ratio b_{\pm}/b_0 according to the relation $\tau_{B^{\pm}}/\tau_{B_d^0} = b_{\pm}/b_0$ as used

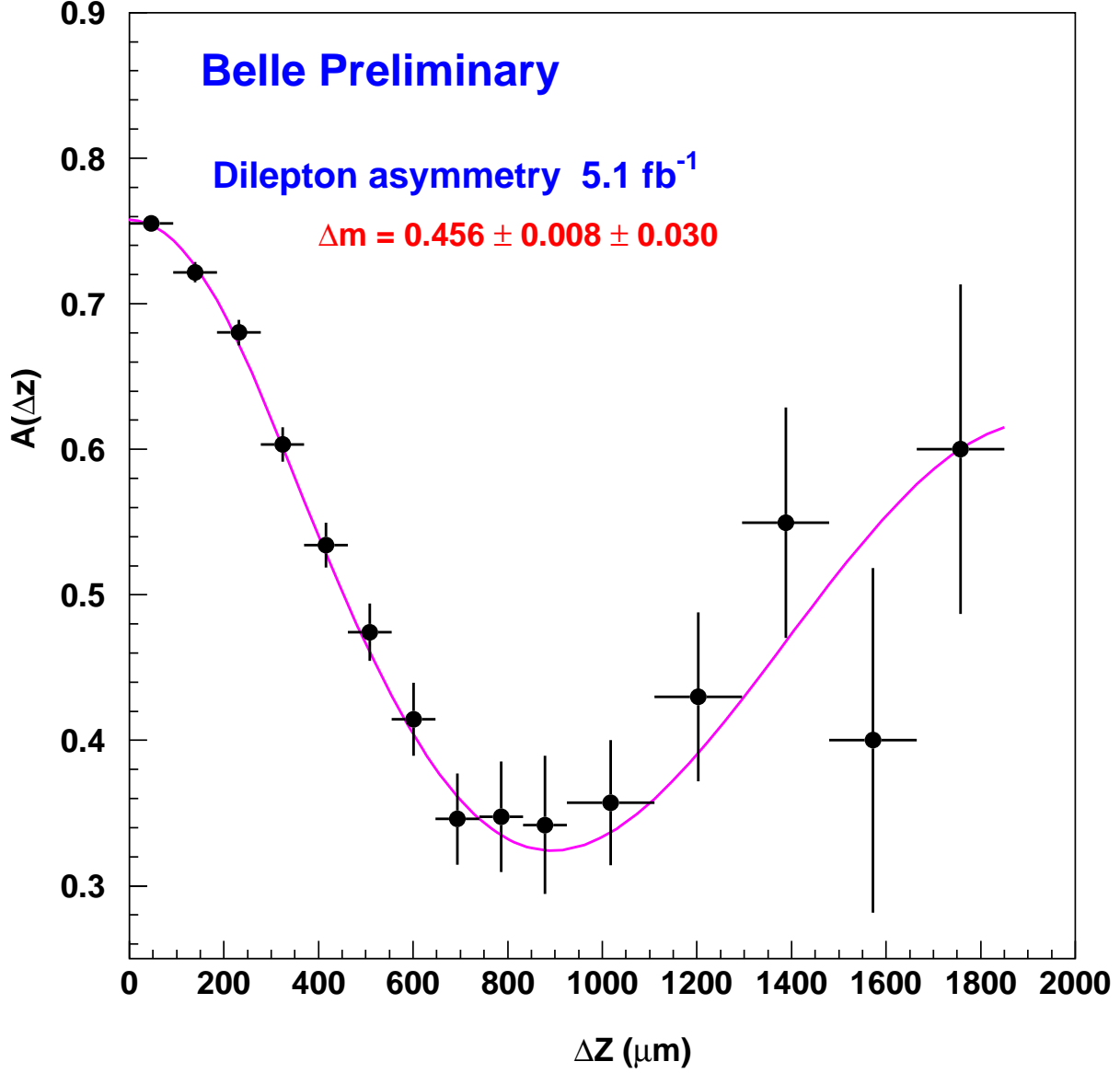


FIG. 7. Opposite and same-sign dilepton asymmetry vs Δz . The asymmetry is defined as $A(\Delta z) = (N_{\text{OS}} - N_{\text{SS}})/(N_{\text{OS}} + N_{\text{SS}})$. The points are the data. The smooth curve is obtained from the Method-II fit functions using the final measured parameters. The binning is different from that of the fit for display purposes.

in the fit. The background composition and distributions were varied in accord with the variation of the indicated parameters.

Response Function

As noted, for this analysis we obtained the response function from the Δz distribution of

dileptons from J/ψ decays in the data sample. The difference between the response function thus obtained and the true dilepton response function introduces a systematic uncertainty. We estimated this uncertainty by repeating the fit using the Monte Carlo dilepton response function with extra smearing as described in Section III E 2.

The statistical uncertainty in the Δz distribution of J/ψ leptons introduces further systematic error. For Method I, we repeated the fits and after varying the number of entries on a bin-by-bin basis by an amount determined by their statistical errors. For Method II, we repeated fits by varying the parameters of double-Gaussian by 1σ .

The proper-time difference calculated using $\Delta t = \Delta z/c\beta\gamma$ is exact only when B -mesons are at rest in the CM frame. The motion of B 's and the energy spread of the accelerator gives additional smearing beyond the response function, which includes only the Δz measurement resolution. The size of this effect was studied using Monte Carlo events. Two fits were performed: one using a response function obtained for the true Δt difference and a second obtained for Δz . Comparing the results we found the shift in Δm_d to be negligible ($\sim 0.001 \text{ ps}^{-1}$).

Errors from the three sources above were summed in quadrature and are listed in Table I.

Background Δz distribution

Since the analysis relies on Monte Carlo simulation of the backgrounds, uncertainties and imperfections in the Monte Carlo simulation lead to uncertainty in the background distributions. The following sources were considered:

Fake rate of lepton-ID: As mentioned above, we find differences in the fake rates of electron- and muon-identification between data and Monte Carlo. These differences, which are of order 10%, are similar in magnitude to the statistical errors in the data-Monte Carlo comparison. To determine the contribution to the overall systematic error from this source, we conservatively assumed a fake-rate uncertainty of $\pm 35\%$ and repeated the fits with the corresponding background variations.

Secondary lepton rates and distribution: The Monte Carlo used in this analysis may not fully describe the B -meson decays to charmed mesons, especially for final states proceeding through higher resonance states and virtual W decays. To determine our sensitivity to such effects, the fits were repeated after varying the branching ratios to D^0 and D^\pm in accord with the experimental uncertainties of CLEO measurements [17]. These changes altered the number and the Δz distributions of secondary leptons in the Monte Carlo-generated background distributions.

Continuum components: The uncertainty of the continuum component includes the ratio of $\Upsilon(4S)$ and continuum events and the uncertainty in continuum event generation by the Monte Carlo. We estimated this uncertainty to be $\pm 10\%$ and repeated the fit after varying the continuum components by this amount.

Uncertainty of detector resolution: As mentioned previously, the Monte Carlo background distributions are smeared to correct for the difference in vertex resolution between that predicted by the Monte Carlo and that observed in the data. The smearing function was a single gaussian with $\sigma = 50 \text{ } \mu\text{m}$. We varied the amount of smearing by the uncertainty ($\pm 18 \mu\text{m}$) in the determination of the extra smearing value and repeated the fit.

Contributions to the systematic error from the above sources are summarized in Table I. The total systematic errors obtained by summing all errors in quadrature are $\pm 0.015 \text{ ps}^{-1}$ and $\pm 0.030 \text{ ps}^{-1}$ for Methods I and II, respectively. Since the results of the two methods

are consistent within errors, we take the value of Method I as the final result. For the systematic error, we conservatively take the larger value of the two methods for each item and add quadratically:

$$\Delta m_d = 0.456 \pm 0.008 \text{ (stat)} \pm 0.030 \text{ (sys)} \text{ ps}^{-1} \text{ (preliminary)}$$

We anticipate that with further study we will be able to reduce the systematic error.

TABLE I. Summary of the systematic errors.

Source (uncertainty)	Method-I	Method-II
f_0/f_{\pm} (1.07 ± 0.09)	± 0.009	± 0.012
B_d^0 life time (1.56 ± 0.04 ps)	± 0.003	± 0.007
$\tau_{B^{\pm}}/\tau_{B_d^0}$ (1.04 ± 0.04)	± 0.010	± 0.022
response function	± 0.004	± 0.011
background fake rate ($\pm 35\%$)	± 0.003	± 0.007
$B \rightarrow D^0 X$ branching fraction ($\pm 4.6\%$)	$< \pm 0.001$	$< \pm 0.001$
$B \rightarrow D^{\pm} X$ branching fraction ($\pm 14.3\%$)	± 0.002	$< \pm 0.001$
continuum components ($\pm 10\%$)	± 0.001	± 0.001
background detector resolution ($\pm 18 \mu\text{m}$)	± 0.002	$+0.000$ -0.007
total	± 0.015	± 0.030

We have also examined the variation of the fit results by varying the cut values of lepton p^* , lepton acceptance, and $\cos\theta_{\ell\ell}^*$ to check for systematic effects not included above. Similarly results obtained from considering ee , $\mu\mu$, and $e\mu$ dilepton events separately were checked. We find that all the variations are consistent with being statistical fluctuations.

IV. SUMMARY

We have measured the $B_d^0\text{-}\bar{B}_d^0$ mixing parameter Δm_d from the time evolution of dilepton yields in $\Upsilon(4S)$ decays using a sample comprising 5.1 fb^{-1} of data. The result is

$$\Delta m_d = 0.456 \pm 0.008 \text{ (stat)} \pm 0.030 \text{ (sys)} \text{ ps}^{-1} \text{ (preliminary)}$$

This result is consistent with the world average value $\Delta m_d = 0.464 \pm 0.018 \text{ ps}^{-1}$. This is the first determination of Δm_d using the time evolution of B^0 -mesons produced in $\Upsilon(4S)$ decays. It demonstrates the capability of measuring time evolution of $B_d^0\text{-}\bar{B}_d^0$ mixing at an asymmetric e^+e^- collider at the $\Upsilon(4S)$, which is an essential ingredient for the measurement of indirect CP asymmetries.

ACKNOWLEDGEMENTS

We wish to express our deep thanks to the KEKB accelerator group for the excellent operation of the KEKB accelerator and their continuous cooperation with the Belle group.

We gratefully acknowledge the help with our computing and network systems provided by members of the KEK computing research center. We thank the KEK and Princeton University machine shop staffs and other technical and engineering staffs for their skillful work in construction and operation of the Belle detector. We acknowledge support from the Ministry of Education, Science, Sports and Culture of Japan and the Japan Society for the Promotion of Science; the Australian Research Council and the Australian Department of Industry, Science and Resources; the Department of Science and Technology of India; the BK21 program of the Ministry of Education of Korea and the Basic Science program of the Korea Science and Engineering Foundation; the Polish State Committee for Scientific Research under contract No.2P03B 17017; the Ministry of Science and Technology of Russian Federation; the National Science Council and the Ministry of Education of Taiwan; the Japan-Taiwan Cooperative Program of the Interchange Association; and the U.S. Department of Energy.

REFERENCES

- [1] LEP B Oscillations Working Group, see <http://www.cern.ch/LEPBOSC/> and references therein.
- [2] CDF Collaboration, F. Abe *et al.*, Phys. Rev. **D60** 072003 (1999); F. Abe *et al.*, Phys. Rev. **D59** 032001 (1998); F. Abe *et al.*, Phys. Rev. Lett., **80** 2057 (1998).
- [3] SLD Collaboration, Kenji Abe *et al.*, Nucl. Instrum. Methods **A446** 53 (2000).
- [4] ARGUS Collaboration, H. Albrecht *et al.* Z. Phys. **C55** (1992) 357; H. Albrecht *et al.* Phys. Lett. **B324** (1994) 249.
- [5] CLEO Collaboration, B. H. Behrens *et al.* CLNS 00-1668, CLEO 00-6 (2000); J. Bartelt *et al.*, Phys. Rev. Lett., **71** 1680 (1993).
- [6] KEKB accelerator group, KEKB B Factory Design Report, KEK Report 95-7, 1995; K. Akai *et al.*, “COMMISSIONING OF THE KEKB B-FACTORY”, WEAR4, Proc. 1999 Particle Accelerator Conference, New York(1999); Y. Funakoshi *et al.*, “KEKB PERFORMANCE”, Proc. 2000 European Particle Accelerator Conference, Vienna(2000).
- [7] BELLE Collaboration, Technical Design Report, KEK Report 95-1, 1995.
- [8] G. Alimonti *et al.*, KEK preprint 2000-34.
- [9] H. Hirano *et al.*, KEK Preprint 2000-2, submitted to Nucl. Instrum. Methods; M. Akatsu *et al.*, DPNU-00-06, submitted to Nucl. Instrum. Methods.
- [10] H. Kichimi *et al.*, submitted to Nucl. Instrum. Methods.
- [11] T. Iijima *et al.*, Proceedings of the 7th International Conference on Instrumentation for Colliding Beam Physics, Hamamatsu, Japan, Nov 15-19, 1999.
- [12] H. Ikeda *et al.*, Nucl. Instrum. Methods **441**, 401 (2000).
- [13] A. Abashian *et al.*, Nucl. Instrum. Methods **A449**, 112 (2000).
- [14] G. Fox and S. Wolfram, Phys. Rev. Lett **41** 1581 (1978).
- [15] Particle Data Group, Review of Particle Physics, The European Physical Journal **C3** (1998).
- [16] CLEO Collaboration, J. P. Alexander *et al.* CLNS 00-1670, CLEO 00-7, hep-ex/00006002, submitted to Phys. Rev. Lett.
- [17] CLEO Collaboration, L. Gibbons *et al.*, Phys. Rev. **D56** 3783 (1997).